Hyperfine Interact
DOI 10.1007/s10751-013-0956-9

Solid solution decomposition and growth of precipitates in Be-Fe alloys from Mössbauer investigations

V. P. Filippov · V. P. Gladkov · S. S. Martynenko · V. I. Petrov

Abstract Mössbauer spectra of fine-grained hot-pressed beryllium and coarse-grained beryllium samples containing different amounts of impurities were obtained after homogenization and after annealing for different durations. Mössbauer spectra of solid solution of iron in beryllium and decomposed during isothermal annealing two different iron containing phases were fitted by a convolution equation of three Lorentz lines. The models of solid solution decomposition and growth of secondary particle precipitates were investigated. The average distance between dislocations and the average grain size were obtained from the application of the models. The dependencies between the decomposition mechanism, the average grain size, the impurity concentrations and the type of the secondary particles precipitates were revealed. The possibility of a coherent analysis of the decomposition process by means of a kinetic law classification and secondary particle precipitates growth processes based on diffusion models has been shown.

Keywords Mössbauer effect · Solid solution · Secondary particle precipitates · Kinetic law · Diffusion models

1 Introduction

Decomposition of an oversaturated solid solution and growth of the secondary particle precipitates (SPP) are typical processes that take place upon thermal treatment of materials. Mössbauer spectroscopy reveals fine details of structure and phase composition [1] which gives information about dissolution and precipitation processes.

The resonant detectors employed in Mössbauer spectrometers make a typical spectral line shape distortion [2]. We considered the possibility of taking into account such

Proceedings of the 32nd International Conference on the Applications of the Mössbauer Effect (ICAME 2013) held in Opatija, Croatia, 1–6 September 2013

V. P. Filippov (✉) · V. P. Gladkov · S. S. Martynenko · V. I. Petrov
National Research Nuclear University, MEPhI, Kashirskoye, 31, Moscow 115409, Russia
e-mail: vpfilippov@mephi.ru

Published online: 19 November 2013

experimental line shape distortion and introduced a mathematical description of the experimentally measured lines [3]. The consideration acceptable under the conditions of no external vibrations, nonlinearity of the operation of the electric circuits in the spectrometer and vibrator, resonance self-absorption in the source, and inhomogeneity of the local atomic and resonant environment of Mössbauer nuclei in the source and the detector. It such a case, the instrument function of the spectrometer is a product of the Lorentz lines of the source and the resonant detector. It was shown that for each equivalent state of the absorber atoms the experimentally detected line χ(E) can be described by a mathematical convolution of three generally different Lorentz lines:

$$\chi(E) = \frac{\Delta_{12}}{\pi^3} \cdot \frac{(E - E_1 - E_3)^2 \Delta_1 \Delta_3 + (E - E_2 - E_3)^2 \Delta_2 \Delta_3 + \delta^2 \Delta_1 \Delta_2 + \Delta_{12} \Delta_{23} \Delta_{13} \Delta_{123}}{\left((E - E_1 - E_3)^2 + \Delta_{13}^2\right)\left((E - E_2 - E_3)^2 + \Delta_{23}^2\right)\left(\delta^2 + \Delta_{12}^2\right)^2}, \tag{1}$$

where E_1, E_2, E_3 are the energies of resonance transitions of the source, detector, and absorber, respectively; $\delta = E_1 – E_2$ is the isomer shift between the source and resonant detector; Δ_1, Δ_2, Δ_3 are the half-widths of the source, detector, and absorber lines, respectively; $\Delta_{ij} = \Delta_i + \Delta_j$, $\Delta_{123} = \Delta_1 + \Delta_2 + \Delta_3$.

We proposed a method of finding the unknown parameters δ, Δ_1, Δ_2 required for fitting the experimental spectra with (1) and carried out a comparative analysis of the fitting quality of the experimental spectra obtained using a resonant detector [4]. It was shown that the fitting of the experimental spectra with (1) describes the experimental lines much better than other techniques.

In this work, Mössbauer spectra of fine-grained hot-pressed beryllium and coarse-grained beryllium samples containing different amounts of impurities were obtained after homogenization and after annealing for different durations. Mössbauer spectra of the solid solution, decomposed during isothermal annealing, and resulting in two different iron containing phases, were fitted by a convolution equation of the three Lorentz lines. Complex spectra containing small intensity doublets and doublets with a small quadrupole splitting were fitted taking into account the spectra distortion. A coherent analysis of the simultaneously proceeding processes was carried out: a) the decomposition of the solid solution according the kinetic law; b) the SPP growth based on the diffusion models that we have previously introduced [5, 6].

2 Experimental technique

Four coarse-grained beryllium alloys with iron content of 0.11–0.32 % (denoted as C1–C4) and five fine-grained hot-pressed beryllium alloys with iron content of 0.12–0.20 % (denoted as HP1–HP5) were prepared (Table 1). The samples for Mössbauer investigations were in the form of plates with a thickness of 2 to 10 mm.

Mössbauer spectrometry was performed at room temperature with a conventional constant acceleration system with a ^{57}Co (in Cr) γ–ray source. Velocity and isomer shift calibrations were performed with reference to sodium nitroprusside at room-temperature. A resonant detector RSDU-2A was used for the γ–ray detection. During the recording of the spectra, the vibrator, the γ radiation source, the detector, and the absorber were placed in a thermostat where a constant temperature of 25.00 ± 0.05 °C was held. Mössbauer spectra of a solid solution of iron in beryllium after homogenization at 1100 °C and spectra with SPP after annealing at 500–600 °C for different durations up to 2000 h were obtained.

Table 1 Analyzed materials

Graphic symbol	Method of preparation	Impurity content, mass %		
		Fe	Al	Sum of Ti, Cr, Mn
C1	Melting of distilled beryllium with the addition of iron in an arc furnace	0.17	0.007	0.019
C2		0.32		
C3	Melting of distilled beryllium with the addition of iron and aluminum in an arc furnace	0.11	0.029	0.067
C4	Melting of technical purity beryllium in an induction furnace	0.15	0.024	0.174
HP1	Hot pressing after the grinding of cast alloys	0.12	0.019	0.040
HP2		0.16	0.024	0.174
HP3		0.16	<0.003	0.136
HP4		0.15	0.024	0.274
HP5		0.20	0.082	0.049

The spectra were fitted by the convolution equation of the three Lorentz lines (1). The fraction of iron in the different phases was determined from the relative area of the phase spectrum.

Figure 1 shows a typical spectrum of the coarse-grained beryllium C1 that was annealed at 560 °C for 1265 h. A typical spectrum of the fine-grained hot-pressed beryllium HP2 annealed at 600 °C for 868 h is shown in Fig. 2. Note that in both cases the result from subtracting the experimental spectrum and the mathematical processing (the difference spectrum) does not exceed the background level.

The process of the solid solution decomposition is usually characterized according the kinetic law described by the Johnson-Mehl-Avrami-Kolmogorov equation [8]:

$$c = \exp(-p \cdot t^n), \tag{2}$$

where c = the relative amount of iron in solid solution at the annealing time t; p = empirical constant; n characterizes the decomposition mechanism (e.g. $n = 2/3$ for segregation to dislocations) and assumes values from 0.5 to 4. If simultaneously proceeding processes occur in a material, they can be described with a following linear combination:

$$c = A_1 \cdot \exp(-p_1 \cdot t) + A_2 \cdot \exp\left(-p_2 \cdot t^{\frac{2}{3}}\right) + A_3 \cdot \exp(-p_3 \cdot t^{3.5}) + A_4. \tag{3}$$

According to the kinetic law classification, the exponents in (3) characterize the following processes respectively: 1) nucleation at the boundaries when other nucleation sites are exhausted; 2) precipitation on dislocations; 3) decomposition at a decreasing rate of nucleation of the new phase. Let A_1, A_2, and A_3 be the relative contributions from the corresponding process to the process of decomposition, and A_4 be a quantity proportional to the limit of impurity solubility in a solid solution at the given annealing temperature so that $A_1 + A_2 + A_3 + A_4 = 1$. The fitting of the experimentally obtained dependence $c(t)$ using (3) can estimate the contributions from different processes. It was found in particular

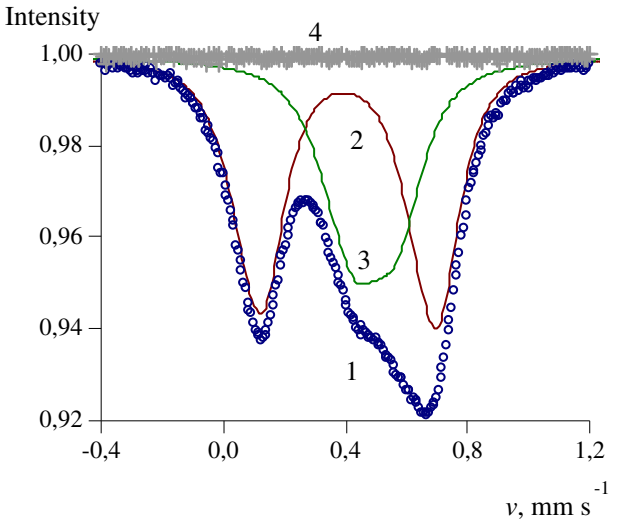

Fig. 1 Spectrum of material C1 upon isothermal annealing at 560 °C for 1265 h: (1) experimental spectrum; (2) mathematical description of solid solution spectrum; (3) mathematical description of $FeBe_x$ phase spectrum; (4) difference spectrum

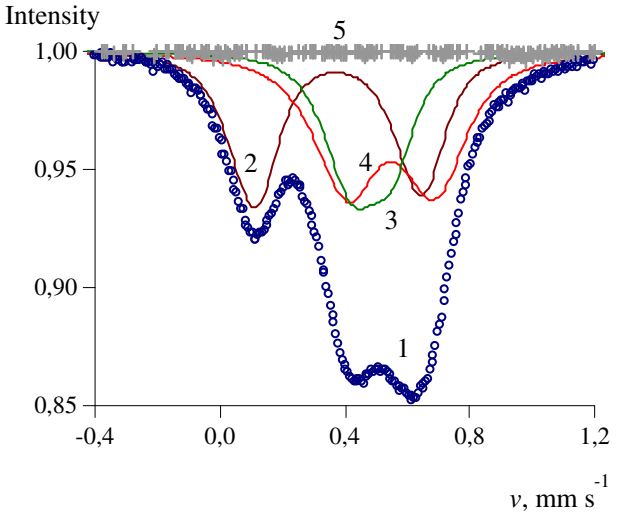

Fig. 2 Spectrum of material HP1 upon isothermal annealing at 600 °C for 868 h: (1) experimental spectrum; (2) mathematical description of solid solution spectrum; (3) mathematical description of $FeBe_x$ phase spectrum; (4) mathematical description of ε phase spectrum; (5) difference spectrum

that the contribution from the process of decomposition to a decreasing rate of nucleation of the new phase is negligible for all of the investigated materials, i.e., $A_3 = 0$.

The process of the SPP growth was analyzed using the models of diffusion from the grain to the boundary and inside the grain as we previously introduced [6] on basis of thermal

Table 2 The diffusion coefficient of iron in beryllium

	D × 10^{14}(cm^2/s)		
	$T = 500\,^{\circ}C$	$T = 560\,^{\circ}C$	$T = 600\,^{\circ}C$
Coarse-cast beryllium	0.097	1.2	5.2
Fine-grained beryllium	0.36	4.1	17.3

conductivity equation solutions [7]. The solution of the diffusion equation from the grain to the boundary in approximation of the spherical grain shape takes the form:

$$c_1 = 1 - 6\pi^2 \sum_{n}^{\infty} \frac{1}{n^2} \exp\left(-\frac{n^2\pi^2 t D}{a^2}\right), \tag{4}$$

here c_1 = the relative amount of iron in the SPP at the grain boundary; t = the annealing time; D = the diffusion coefficient of iron in beryllium at the corresponding annealing temperature; a = the average grain size. Summation with respect to n carries from 0 to 50.

In considering the diffusion equation inside the grain, the set of microstructure flaws serving as a sink for impurities was approximated by alternating parallel plate-like nanoformations (dislocations). In this case, the solution of the diffusion equation takes the form:

$$c_2 = 1 - \frac{8}{\pi^2} \sum_{n}^{\infty} \frac{1}{(2n+1)^2} \exp\left[-\frac{(2n+1)^2\pi^2 t D}{L^2}\right], \tag{5}$$

here c_2 = the relative amount of iron in the SPP on the nanoformation plates inside the grain; L = the average distance between layers of the nanoformation plates. Summation with respect to n carries from 0 to 90. The diffusion coefficient of iron in beryllium D at the corresponding annealing temperature T was calculated by extrapolation of the data obtained by the radiography for the temperature range of 920−1120 °C [9] (Table 2).

Let c^i be the relative amount of iron in the ith secondary precipitated phase ($i = 1, 2$) so that:

$$c + \sum_{i} c^i = 1, \tag{6}$$

i.e., the sum of the relative amount of iron in the solid solution c and in the SPP phases c^i is equal to one during the annealing. The experimentally obtained dependencies $c^i(t)$ were approximated by the sum of the processes (4) and (5):

$$c^i(t) = k_1^i \cdot c_1(t) + k_2^i \cdot c_2(t), \tag{7}$$

here k_1^i, k_2^i = the relative contributions to the SPP growth from the processes (4) and (5), respectively. The solution with respect to k_1^i, k_2^i, A_1, A_2, A_3, A_4 was found along with the conditions

$$A_1 = \sum_{i} k_1^i;\ A_2 = \sum_{i} k_2^i, \tag{8}$$

i.e., the total contribution from the precipitation of all secondary phases onto plate-like formations according the solution of the diffusion equation is equal to the contribution to the decomposition of the solid solution on dislocations according the kinetic law classification; the total contribution from the precipitation of all secondary phases to the grain boundary according the solution of the diffusion equation is equal to the contribution to the decomposition of the solid solution on the grain boundary according the kinetic law classification. Thus, a consistent solution for the models of the solid solution decomposition based on the

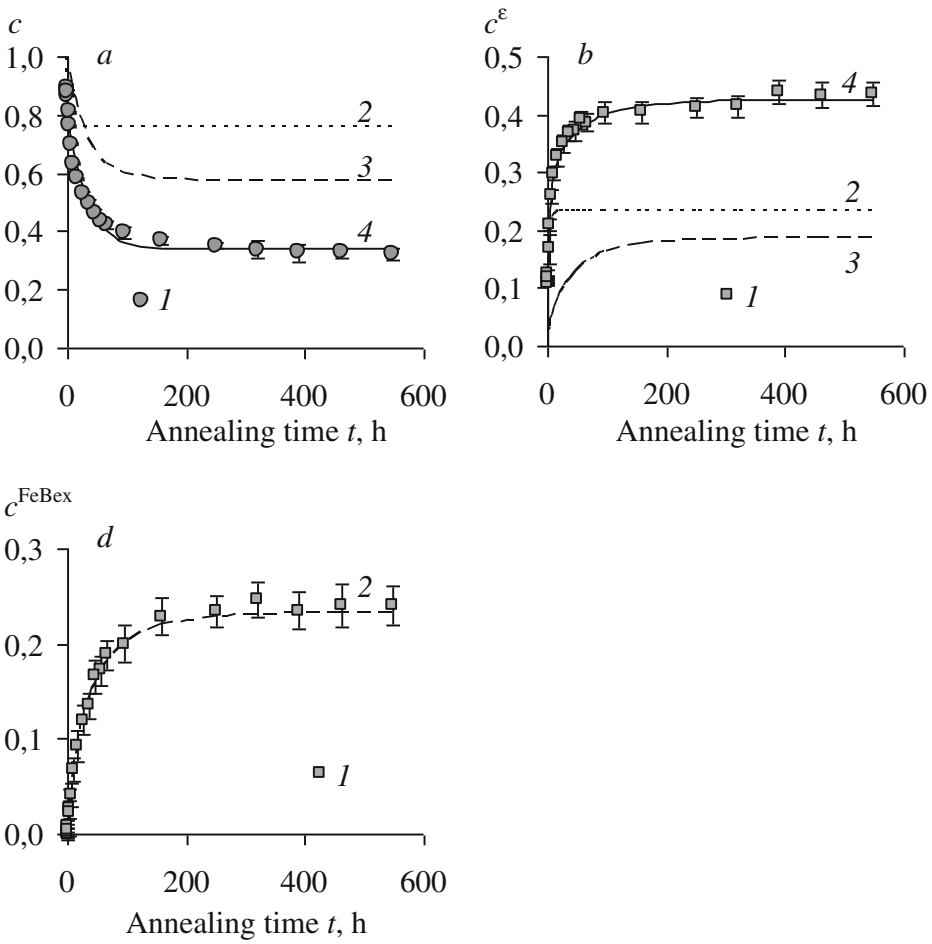

Fig. 3 Material HP2 upon isothermal annealing at 600 °C. **a** (1) the relative amount of iron in solid solution; (2) precipitation on dislocations; (3) nucleation at grain boundaries; (4) total decomposition process. **b** (1) the relative amount of iron in ε phase; (2) precipitation on dislocations; (3) precipitation at grain boundaries; (4) total precipitation process. **d** (1) the relative amount of iron in $FeBe_x$ phase; (2) precipitation at grain boundaries, i.e. total precipitation process

kinetic law classification and the diffusion growth of the SPP based on the solution of the diffusion equation was found.

The consistent dependences of the relative amount of iron in the solid solution and in the secondary phases in the HP2 material on the length of annealing at a temperature of 600 °C are shown in Fig. 3.

3 Discussion

For all of the investigated materials, two SPP phases could be determined according to the consistency of the Mössbauer parameters (Table 3): $FeBe_x$ [10, 11] and $AlFeBe_m$ (the most likely $m = 4$) [11, 12].

Table 3 Coefficients of the consistent solution for the models of the solid solution decomposition according the kinetic law classification and the diffusion growth of the SPP according the diffusion equation solution; Mössbauer characteristics of iron-containing phases, mm·s^{-1}

Graphic symbol	T_{anneal}, °C	t_{inc}, h	Decomposition according to kinetic law			Diffusion growth				Solid solution of Fe in Be			$FeBe_x$ phase			Phase ε		
			A_1	A_2	A_4	k_1^{FeBex}	k_2^{FeBex}	k_1^{ε}	k_2^{ε}	Is	Qs	Γ	Is	Qs	Γ	Is	Qs	Γ
C1	560	~0	0	0.82	0.18	0	0.82	–	–	0.43	0.57	0.10	0.51	0.15	0.13	–	–	–
C1	560	~0	0	0.74	0.26	0	0.74	–	–	0.43	0.57	0.10	0.51	0.14	0.14	–	–	–
C2	500	82	0	0.88	0.12	0	0.88	–	–	0.43	0.57	0.10	0.50	0.12	0.16	–	–	–
C3	560	51	0	0.42	0.58	0	0.19	0	0.23	0.42	0.57	0.12	0.50	0.14	0.20	0.65	0.35	0.19
C4	600	78	0	0.45	0.55	0	0.12	0	0.33	0.42	0.56	0.10	0.52	0.12	0.12	0.58	0.35	0.15
HP1	600	~0	0.20	0.45	0.35	0.12	0.06	0.08	0.39	0.41	0.54	0.10	0.50	0.14	0.10	0.58	0.28	0.14
HP2	600	~0	0.42	0.24	0.34	0.23	0	0.19	0.24	0.40	0.53	0.10	0.50	0.13	0.10	0.57	0.28	0.16
HP2	560	10	0.46	0.54	0	0.32	0.11	0.14	0.43	0.40	0.53	0.10	0.50	0.12	0.10	0.57	0.27	0.17
HP2	500	10	0.39	0.61	0	0.39	0.03	0	0.58	0.40	0.52	0.10	0.50	0.13	0.10	0.56	0.27	0.19
HP3	600	~0	0.36	0.46	0.18	0.31	0.18	0.05	0.28	0.42	0.57	0.10	0.54	0.17	0.14	0.58	0.34	0.16
HP3	560	~0	0.40	0.44	0.16	0.40	0.28	0	0.16	0.42	0.57	0.10	0.52	0.15	0.13	0.56	0.30	0.16
HP4	560	~0	0.48	0.34	0.18	0.48	0.25	0	0.09	0.42	0.57	0.10	0.52	0.16	0.14	0.58	0.32	0.14
HP5	600	~0	0.35	0.35	0.30	0.35	0.09	0	0.26	0.40	0.54	0.10	0.51	0.13	0.12	0.57	0.31	0.16
HP5	560	8	0.49	0.25	0.26	0.49	0	0	0.25	0.41	0.54	0.11	0.51	0.13	0.12	0.57	0.30	0.16
HP5	500	60	0.73	0.27	0	0.73	0	0	0.27	0.42	0.54	0.10	0.51	0.12	0.12	0.57	0.30	0.19
Error			±0.05							±0.02 mm·s^{-1}								

The spectrum of the $FeBe_x$ phase is a doublet with quadrupole splitting of 0.13 ± 0.02 mm·s^{-1} consisting of two equal lines. In Figs. 1 and 2, however, a noticeable asymmetry of the mathematical description of the $FeBe_x$ phase can be seen. As noted earlier, the instrument function of the spectrometer with a resonant detector is a product of the Lorentz lines of the source and the resonant detector, thus it is generally asymmetric. Therefore all of the spectrum lines are generally asymmetric, and the doublet which is a superposition of two equal lines becomes asymmetric too. Fitting the experimental spectra using (1) allows us to take these distortions into account.

It was found that the relative amount of iron precipitated in the $FeBe_x$ phase was from 12 to 88 % for the coarse-cast materials and from 18 to 73 % for the fine-grained materials, that apparently depends on the impurity composition but not the average grain size. The $FeBe_x$ phase precipitates mainly on the grain boundaries in the fine-grained materials. In the coarse-cast materials, the $FeBe_x$ phase precipitates on the dislocations, no precipitation of the $FeBe_x$ phase was detected at the grain boundaries.

The existence of the incubation period t_{inc} was confirmed [6]. The presence and the duration of the incubation period depend on the annealing temperature, the secondary phase type, and apparently the impurity composition. For the $FeBe_x$ phase, it lasted from 10 to 82 h at the annealing temperature of 500 °C. The incubation period increases with a decrease of the annealing temperature.

It was found that the phase with isomer shift and quadrupole splitting close to that of $AlFeBe_4$ precipitates without incubation period both in aluminum-enriched materials (Table 1) and in the materials characterized by a lower concentration of aluminum but containing other impurities. The relative amount of iron precipitated in this phase in the HP2 material was 58 %. At the same time, this phase does not precipitate in C1 and C2 samples with much lower concentrations of Al, Ti, Cr, and Mn impurities. Based on the above, we conditionally denote this phase as ε, assuming that its composition is complex even though it is close in its Mössbauer characteristics to $AlFeBe_4$. Phase ε precipitates mainly on the dislocations regardless of the average grain size.

In the example shown in Fig. 3, the $FeBe_x$ phase precipitated only on the grain boundaries, the ε phase precipitated on both the grain boundaries and the dislocations.

For the coarse-cast materials, the average grain size was assumed to be 1 mm, while the estimated distance between dislocations was from 0.8 to 8.1 μm. For the fine-grained materials, the estimated average grain size was from 6 to 20 μm, the estimated distance between dislocations was from 0.6 to 1.7 μm.

We hope the obtained results will be useful in analyzing SPP growth and solid solution decomposition processes in the thermal treatment and use of beryllium materials.

4 Conclusion

The spectra obtained with the use of resonant detectors must be fitted taking into account the typical line shape distortion and the instrumental function asymmetry. The convolution equation of the three Lorentz lines is recommended to be used.

The possibility of a coherent analysis of the decomposition process by means of kinetic law classification and SPP growth processes based on diffusion models has been shown. The analysis was performed according to data obtained with using of Mössbauer spectroscopy. The average grain size and the distance between dislocations could be estimated from the analysis.

In the beryllium alloys with 0.11–0.32 % Fe the phase $FeBe_x$ decomposes with an incubation period, which increases with decreasing annealing temperature. The $FeBe_x$ phase precipitates mainly on the grain boundaries in the fine-grained materials and on the dislocations in the coarse-cast materials.

In the alloys with noticeable impurities of Al, Ti, Cr, Mn group, in addition to phase $FeBe_x$, a phase with Mössbauer spectra parameters similar to those of the compound $AlFeBe_4$ precipitates mainly on the dislocations without incubation period.

The mechanism of the SPP growth depends on the average grain size and the impurity composition.

References

1. Goldanskii, V.I., Herber, R.H.: Chemical Applications of Mössbauer Spectroscopy. Acad Press, London (1968)
2. Petrov, V.I., Filippov, V.P., Shikanova, Yu.A.: Messbauerovskaya Spektroskopiya i ee primeneniya. Sbornik tezisov dokladov 10-i mezhdunarodnoi konferentsii (Proc. 10th Int. Conf. Mössbauer Spectroscopy and Its Applications). Izhevsk: Ural Branch Russ. Acad. Sci. 74 (2006)
3. Gladkov, V.P., Martynenko, S.S., Petrov, V.I.: Zh. Prikl. Spektrosk **78**(2), 316–320 (2011)
4. Gladkov, V.P., Petrov, V.I., Martynenko, S.S., Kryanev, A.V.: Yad. Fiz. Inzh **3**(4), 1–7 (2012)
5. Gladkov, V.P., Dubinskaya, Y.L., Rumyantsev, I.M.: Perspektivnye materialy. Spetsial'nyi vypusk: sb. trudov Pyatoi rabochei gruppy Mezhdunarodnogo energeticheskogo agenstva po berilliyu (Promising Materials. Special Issue. In: Proceeding of the 5th Working Group of International Energy Agency on Beryllium), pp. 65–69. Interkontakt Nauka, Moscow (2002)
6. Vishnyakova, T.V., Goncharenko, M.S., Petrov, V.I., Taranov, K.V.: Bull. Russ. Acad. Sci. Phys **74**(3), 399–401 (2010)
7. Carslaw, H.S., Jaeger, J.C.: Conduction of Heat in Solids. Oxford University Press, London (1959)
8. Cahn, R.W., Haasen, P.: Material Science and Technology. VCH, Weinheim (1991)
9. Gladkov, V.P., Petrov, V.I., Rumyantsev, I.M.: Atom. Energy **98**(2), 146–149 (2005)
10. Janot, C., Gibert, H.: Mater. Sci. Eng **10**(1), 23–31 (1972)
11. Papirov, I.I.: Struktura i svoistva splavov berilliya. Spravochnik (Structure and Properties of Beryllium Alloys. Handbook). Energoatomizdat, Moscow (1981)
12. Belozerskii, G.N., Grigor'ev, A.K., Ivanov, V.A., Semenov, V.G., Sokolov, A.Y., Aleksandrov, A.A.: Pis'ma Zh. Tekh. Fiz **13**(9), 531 (1987)